Constrained Statistical Modelling of Knee Flexion from Multi-Pose Magnetic Resonance Imaging

Mihaela A.M. Constantinescu, Su-Lin Lee, Nikhil V. Navkar, Weimin Yu, Saifedeen Al-Rawas, Julien Abinahed, Guoyan Zheng, *Member, IEEE*, Jennifer Keegan, Abdulla Al-Ansari, Nabil Jomaah, Philippe Landreau and Guang-Zhong Yang, *Fellow, IEEE*

***Abstract*—Reconstruction of the anterior cruciate ligament (ACL) through arthroscopy is one of the most common procedures in orthopaedics. It requires accurate alignment and drilling of the tibial and femoral tunnels through which the ligament graft is attached. Although commercial computer-assisted navigation systems exist to guide the placement of these tunnels, most of them are limited to a fixed pose without due consideration of dynamic factors involved in different knee flexion angles. This paper presents a new model for intraoperative guidance of arthroscopic ACL reconstruction with reduced error particularly in the ligament attachment area. The method uses 3D preoperative data at different flexion angles to build a subject-specific statistical model of knee pose. To circumvent the problem of limited training samples and ensure physically meaningful pose instantiation, homogeneous transformations between different poses and local-deformation finite element modelling are used to enlarge the training set. Subsequently, an anatomical geodesic flexion analysis is performed to extract the subject-specific flexion characteristics. The advantages of the method were also tested by detailed comparison to standard Principal Component Analysis (PCA), nonlinear PCA without training set enlargement, and other state-of-the-art articulated joint modelling methods. The method yielded sub-millimetre accuracy, demonstrating its potential clinical value.**

***Index Terms*—Magnetic resonance imaging (MRI), Atlases, Image-guided treatment, Probabilistic and statistical methods, Shape analysis, Surgical guidance.**

I. Introduction

ANTERIOR cruciate ligament (ACL) reconstruction is a common orthopaedic procedure. In the UK, it accounts for 40 % of all sports-related injuries [1]. An ACL injury typically occurs when there is a violent twist or hyperextension of the knee, with ACL-deficiency associated with an increased rate of degenerative changes and meniscal injuries. The ACL reconstruction surgery consists of the replacement of the knee ligament with a graft inserted via tunnels drilled through the tibia and femur. The surgery is performed using arthroscopy in a minimally invasive fashion and successful clinical outcome depends upon the structural and functional accuracy while placing the tunnel [2].

Currently commercially available computer-assisted navigation systems for orthopaedic procedures such as KneeNav [3], OrthoPilot [4], CASPAR [5], and BrainLab [6] involve extensive user input and rely on optical markers requiring a direct line of sight. In addition, they often require manual registration, which is a time-consuming process exacerbated when using several anatomical landmarks. Furthermore, the osseous fixation of reference arrays is an invasive process and may lead to complications [7]. Therefore, given these technical challenges, there is a need for accurate real-time 3D visualisation of the surgical field, including ligaments, tendons, and the surrounding anatomical structures with due consideration of different flexion positions. In particular, the system should offer increased value by reducing the amount of operator input and the invasiveness to the patient.

In this paper, we propose to minimise the invasiveness of intraoperative tracking of the knee pose by incorporating preoperative information about the shape and the motion range of the knee bones. This information can be integrated into a statistical model and then used to train the algorithm to match to new flexions during the procedure when the knee is bent at different angles for better access. The parameterised anatomic model can subsequently be overlaid on the arthroscopic camera view to enhance the visualisation of structures in the field-of-view and to improve orientation at the surgical site. In addition, the intraoperative statistical model of flexion can simulate the range of motion of the repaired joint by using patient-specific data. The statistical model built previously from ACL-torn knee scans can be updated with intraprocedural arthroscopic images. Finally, a dynamically fitted flexion model can be used as a virtual fixture for an arthroscopic robot to avoid damaging surrounding soft tissue.

Since their introduction by Cootes *et al.* [8], statistical shape models (SSMs) have been a popular method for mathematically expressing not only shape, but also pose variations. The pose instantiation ability of statistical modelling suggests its potential use in tracking the bones subject to rigid transformations during knee flexion. This approach will be pursued in this work.

For tracking the pose of known objects, in the early years, Stark and Fuchs approached the problem in two steps. They

M.A.M. Constantinescu, S.-L. Lee, and G.-Z. Yang are with the Hamlyn Centre for Robotic Surgery, Imperial College London, SW7 2AZ London, UK e-mail: g.z.yang@imperial.ac.uk

N.V. Navkar, S. Al-Rawas, and J. Abinahed are with the Qatar Robotic Surgery Centre, Qatar Science & Technology Park, Doha, Qatar.

W. Yu and G. Zheng are with the Institute for Surgical Technology and Biomechanics, University of Bern, 3014 Bern, Switzerland

J. Keegan is with the Cardiovascular Biomedical Research Unit, Royal Brompton Hospital, SW3 6NP London, UK

A. Al-Ansari is with the Urology Department, Hamad General Hospital, Doha, Qatar.

N. Jomaah and P. Landreau are with the Aspetar Orthopaedic and Sports Medicine Hospital, Doha, Qatar.

first applied an active contour model [9] extended with a shape-change predicting Kalman filter, followed by a pose estimation from the 2D outline rotation and translation [10]. Combination of shape and pose estimation was performed in a maximum *a posteriori* framework [11] in an iterative process. Models for ACL reconstruction were first developed as early as 1999 [12]. Intraoperative instantiation based on a small patch on the femur was the final guidance goal. The method was tested both on simulated and real intraoperative data. Knee motion was taken into consideration only later [13]; a SSM of knee kinematics was fitted intraoperatively from fluoroscopic images, obtaining submillimetre accuracy. Recently, particular interest has been directed to multi-object SSM in orthopaedic procedures. In [14], Fitzpatrick *et al*. built a 3D model of the patella and femur from MRI. Mechanical flexion was also integrated in a joint shape-pose vector and its performance was compared to a finite element model.

More recently, an articulated SSM (aSSM) was developed in order to reconstruct the 3D surface of a hip joint from 2D X-ray [15]. The preservation of the relationship between neighbouring structures was achieved by estimation of the rotation parameter of the femur around the joint centre from a given X-ray. The statistical analysis was only applied to the pose-invariant bone surfaces. Qualitative testing of the bone intersection was performed. Despite being fast and not needing training data, the alignment method proposed here relied on a rotation of the femur about a single axis in the rigid hip structure. Although this method is applicable to knee flexion, i.e. the tibia and patella rotating about a fixed axis in the femur, it does not account for twisting in secondary axes and can lead to significant alignment error.

From a mathematical point of view, the knee flexion is a complex pose variation of the bone surfaces, which cannot be described by a linear function of the degrees of freedom of the joint components. Thus far, several methods have been proposed to mitigate this problem. Neural networks were used to fit nonlinearly distributed data in one of the first attempts at a so-called nonlinear PCA [16]. The learning followed hierarchical steps and combined the discrimination between components with a multi-layer auto-associative perceptron. The author reported increased classification accuracy with a lower number of components.

Later on, Principal Geodesic Analysis (PGA) [17] and its variant Principal Arc Analysis (PAA) [18] were developed. Fletcher *et al.* [17] built on the PCA's limitation to geometric models of landmarks or of dense contour points only and developed a method for nonlinear Riemannian symmetric spaces, including medial representations or parameters of affine transformation matrices. They used the algorithm to describe the variability of fibre orientation in diffusion tensor MRI. Later, it was applied on joint pose+shape models of brain formations [19]. In their work, the pose and shape vectors were concatenated and variance-based weights were applied to balance the principal components. The method demonstrated improved results compared to a pure shape model. Another finding was that pose+shape models had a much smaller model size than simple shape models. A probabilistic framework was added to PGA and the new method was validated against simulated sphere data and real brain models [20]. Compared to PCA on Riemannian data and least-squares (standard) PGA, probabilistic PGA yielded better accuracy. Using PAA, data following nongeodesic arcs on a sphere was modelled as described in [18]. After mapping the points onto a linear space, PCA was applied and the principal components were back-projected onto the original manifold. Their method was validated on medial representations and showed improved results when compared with PAA, PGA, and PCA.

In order to improve the instantiation abilities of a model built with a small number of samples, artificial enlargement of the training set is often performed. One of the first approaches is the combination of SSMs with finite element analysis [21], where the finite element method is applied to shapes in the original training set to generate additional local deformations. Another training set enlargement approach is based on an adaptive focus. The algorithm first locks onto the most reliable structures and then progresses in the hierarchical framework to model the rest of the shapes [22]. Finally, the training set can also be enlarged by different quantification of the wavelet transform coefficients [23]. These methods, alongside non-rigid scaling, non-rigid movement, and noising, were tested in a comparative study on cardiac images, with the non-rigid deformation methods performing best [24]. Non-rigid movement was consequently described in more detail and applied for better image segmentation [25]. In the context of arthroscopic ACL repair, artificial training set enlargement is important because of the limited number of datasets acquired preoperatively in the clinical setting. In preparation for the procedure, the knee may be scanned at as few as four flexion angles. This results in a small training set which renders the modelling of the motion range and the prediction about intraoperative knee poses difficult.

This paper offers a novel addition to the traditional intra-operative tracking for ACL reconstruction by using a pre-operative atlas of knee flexion. The research in this article covers the preoperative model building and involves a new combination of anatomic geodesic decomposition of a training set previously enlarged with a new set of piece-wise rigid transformations. The complexity of the knee flexion, described mathematically through a nonlinear function of the transformation parameters, is circumvented by the application of PCA in the manifold of the parameters themselves, rather than on the anatomy contours. The results show good accuracy and render the method potentially applicable in clinical scenarios.

Data from four flexion angles of twenty intact ACL subjects will be used to generate twenty patient-specific models of flexion based on nonlinear PCA. The statistical analysis is performed on an extended training set enlarged from the four initial flexion shapes by local changes in the flexion parameter vector. For additional quantitative validation, a knee phantom was scanned at the four flexion positions similarly to the human subjects. Moreover, we added three new poses of the phantom which were not included in the training set. Finally, the phantom was also scanned at twelve combined flexion and twisting angles to test the accuracy in modelling secondary knee motion. In total, eighty-four cross-validation studies and three blind validation tests on three intermediate

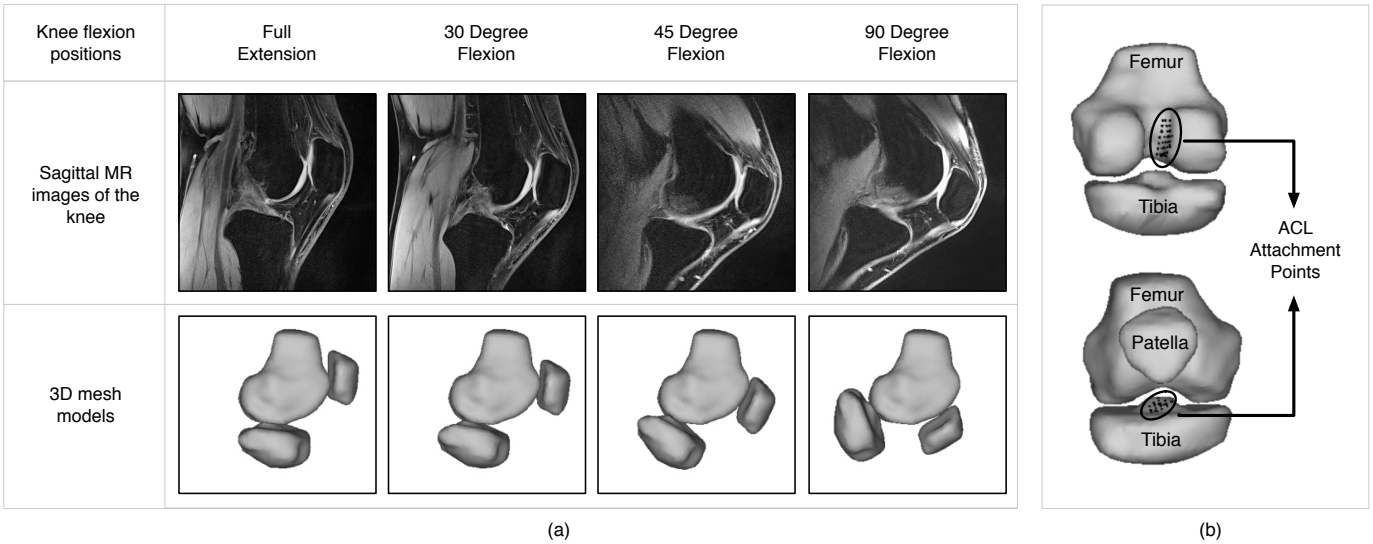

Fig. 1. (a) Flexion data set for a single patient. (b) ACL attachments on the femur and the tibia for one subject, meshes in full extension. The 3D attachment point vector was defined as the concatenation of attachment areas for all flexion angles. A bone vertex belonged to the attachment area if it was within 1 mm from any ACL vertex.

flexion angles, as well as twelve studies of the twisting model were conducted, with the outcome detailed in the Results and Discussion sections. Our method was compared to the state-of-the-art in articulated shape models [15] to demonstrate its relative merit and potential pitfalls.

II. Material and Methods

A. Experimental Setup

The proposed method was tested on MR datasets of the knee collected from twenty healthy volunteers with intact ACL, as well as on CT images of a knee phantom. Seven of the subjects were recruited at Qatar Robotic Surgery Centre (Doha, Qatar) and Aspetar Orthopaedic and Sports Medicine Hospital (Doha, Qatar). The remaining thirteen subjects were scanned at the Biomedical Research Unit (BRU), Royal Brompton Hospital (London, UK). Written informed consent was signed by all subjects, in accordance with local ethics guidelines.

The first seven data sets were collected with a 1.5 T Siemens Espree MRI device, while for the subsequent thirteen, a 3 T Siemens Skyra machine was used. In both cases, a 3D Dual Echo Steady State (DESS) sequence (TR/TE 14.8 ms/5.1 ms) under the Water Excitation imaging protocol was run (flip angle 25 degrees). The subjects were scanned at four flexion positions: full extension, 30 degrees, 45 degrees, and 90 degrees (Fig. 1). The angles were measured with respect to the full extension (0 degrees), as in the case of natural anatomical knee flexion, and the values were taken from orthopaedic diagnostic literature [26], [27], [28].

The MR images (Pixel size = $0.46\times0.46\,\text{mm}^2$; FOV = $150\times150\,\text{mm}^2$; Slice thickness = 3 mm; Inter-slice thickness = 3 mm for the 1.5 T scan and Pixel size = $0.7\times0.7\,\text{mm}^2$; FOV = $169\times180\,\text{mm}^2$; Slice thickness = 0.6 mm; Inter-slice thickness = 0.6 mm for the 3 T scan, respectively) were oriented transversely to capture the anatomy 5 cm underneath the tibial notch to 5 cm above the femoral condyles to ensure

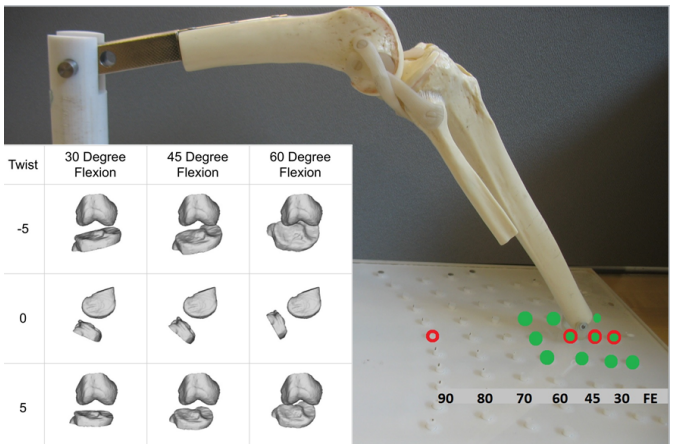

Fig. 2. Experimental setup for scanning the knee phantom. For cross-validation of the enlarged training set knee flexion model, scans of the knee in full extension (FE), 30, 45, and 90 degrees flexion (red circles) were acquired. Additionally, the knee was scanned in 60 degrees flexion and 5 degrees twisting either side of the normal tibia axis in full extension, 30, 45, and 60 degrees flexion (green points). This was done in order to validate the method for simultaneously flexed and twisted knees.

inclusion of patella and ACL. An expert manually delineated the first seven datasets in OsiriX [29] and the additional thirteen in Analyze 10.0 (AnalyzeDirect, Overland Park, KS). The delineated boundaries of the tibia, femur, patella, and ACL were used to segment the images into binary masks. The binary masks were fed to the marching cubes algorithm [30] followed by a Laplacian smoothing filter [31] to generate 3D models of the knee structures as triangular meshes. Finally, the meshes were smoothed using the Poisson reconstruction in MeshLab [32].

For validation, a CLA 10 knee phantom (Coburger Lehrmittelanstalt, Coburg, Germany) comprising of femur, tibia, and ligaments, was scanned using cone-beam CT in a Innova 4100 (GE Healthcare, Little Chalfont, Buckinghamshire, UK) in

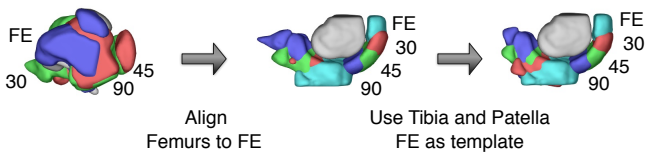

Fig. 3. Alignment of the mesh in the preprocessing step. For each subject, all femurs in flexion poses were aligned to the full extension mesh. Subsequently, the transformations of patella and tibia in full extension to the other angles were computed. These two meshes were used as templates for the final rendering on the right.

full extension, 30, 45, and 90 degrees flexion. The board with the flexion marks is depicted in Fig. 2. The knee was scanned in 5 degrees twisting either side of the tibial axis in full extension, 30, 45, and 60 degrees flexion. The 5 degree twisting was chosen to be within the normal range of motion of a healthy subject [33], which is up to 10 degrees, but this was also limited in the setup by the mobility of the plastic knee phantom. This data was acquired in order to test the method on simultaneously flexed and twisted knees. The femur, tibia, and ACL were segmented and their surfaces were extracted using Analyze 10.0 and smoothed in MeshLab.

B. Data Preprocessing

In this study, the orientation of the femur for each subject was considered fixed throughout the knee flexion. The data preprocessing comprised of two steps of mesh alignment. Graphically, these are summarised in Fig. 3. The femur meshes at 30, 45, and 90 degree flexion were registered to the femur mesh at full extension using Iterative Closest Point (ICP) [34] in MeshLab. The femur mesh at full extension was kept as the subject-specific femur surface from this point on.

Using the femur alignment matrices computed in the aforementioned step, the remaining meshes, comprising of patella, tibia, and ACL at 30, 45, and 90 degrees flexion, were subsequently transformed into the full extension coordinate frame. The transformation matrices of the patella and tibia in full extension to the other three angles were determined by ICP, yielding six homogeneous transformation matrices. The meshes of the knee structures at full extension were used as templates and transformed to the other poses using the homogeneous matrices computed with ICP (Fig. 3).

Along with the transformation of the bones (patella, tibia, and femur), the ACL mesh was also transformed. The ACL attachment points were determined as the vertices on the femur and tibia meshes located within 1 mm proximity of the vertices of the ACL mesh (Fig. 1). For each subject, this represented two sets of sparse points, one on the femur and one on the tibia. Because of the assumption of fixed femur, the movement of the femoral ACL attachment points was neglected in this paper.

To generate the statistical model of flexion, a template of the surface vertices in full extension was established from which the other poses originated. The rigid transformations moving the knee to the other three angles were computed with a simple formulation of Horn's algorithm [35] based on Singular Value Decomposition (SVD) and orthonormal matrices that determine the translation of the centre of mass and subsequently the rotation.

C. Statistical Model of Flexion

The flexion from full extension to any other angle was mathematically described through the homogeneous matrix which rigidly transformed the surface of the patella or the tibia to another flexion angle:

$$\mathbf{T} = \begin{bmatrix} \mathbf{R} & \mathbf{t} \\ \mathbf{0} & 1 \end{bmatrix} \tag{6}$$

where $\mathbf{R}$ was the rotation matrix (Eq. (7), with $c = cos$ and $s = sin$), $\mathbf{t} = [t_\mathrm{x}, t_\mathrm{y}, t_\mathrm{z}]^\mathrm{T}$ the translation vector, and $\mathbf{0} = [0,0,0]$.

It was assumed that the patella and the tibia were moved according to two independent transformation laws; thus, three transformation matrices were computed to align the bones of each subject, from full extension to each of the other angles. Each rigid transformation matrix had six parameters describing the three independent translations and three independent rotations possible in the geometric space. Each flexion was therefore fully described by the concatenated transformation parameters of both patella and tibia matrices.

Extending Cootes's shape analysis [8] and Fletcher's geodesic analysis [17], a statistical analysis was performed on the concatenated vector of rigid transformation parameters, analogous to Cootes's shape vector. The transformation parameters described an anatomical geodesic of knee flexion angles.

For each subject, the data set comprised four observations of the random variable $\mathbf{p}$, one measurement $\mathbf{p}_{f,s} = [\alpha_{f,s}; \beta_{f,s}; \gamma_{f,s}; t_{\mathrm{x},f,s}; t_{\mathrm{y},f,s}; t_{\mathrm{z},f,s}]$ for each flexion pose $f \in Flexion$ = {FE,30,45,90} and for each structure $s \in Structure$ = {Patella,Tibia}. Therefore, $\mathbf{p}_f$ was the concatenated vector of rigid transformation parameters, with α, β, and γ the rotation angles about the global x, y, and z axes and $t_\mathrm{x}, t_\mathrm{y}, t_\mathrm{z}$ the translation parameters. The vectors $\mathbf{p}_f$ spanned a 12-dimensional linear space where the random variable followed a Gaussian distribution (as proved by Kolmogorov-Smirnov tests for every cross-validation training set, with significance level 5 %), thus allowing for linear PCA to be applied. Moreover, $\mathbf{p}$ was the input of the embedding function $\mathbf{\Phi}$: $M \rightarrow \mathbb{R}^{(n_\mathrm{Patella}+n_\mathrm{Tibia})\times 3}$ which took the manifold M, $\mathbb{R}^{12}$ in this case, to the 3D Cartesian space of $n_\mathrm{Patella} + n_\mathrm{Tibia}$ vertices: $\mathbf{\Phi}(\mathbf{p}_f) = [\phi(\mathbf{p}_{f,\mathrm{Patella}})^\mathrm{T}, \phi(\mathbf{p}_{f,\mathrm{Tibia}})^\mathrm{T}]^\mathrm{T}$, with

$$\phi(\mathbf{p}_{f,s}) = \mathbf{T}(\alpha, \beta, \gamma, t_\mathrm{x}, t_\mathrm{y}, t_\mathrm{z})_{f,s} \cdot [\mathbf{x}_{\mathrm{FE},s}; \mathbf{y}_{\mathrm{FE},s}; \mathbf{z}_{\mathrm{FE},s}; \mathbf{1}].$$

$$\mathbf{R} = \begin{bmatrix} c(\alpha)c(\beta) & -c(\beta)s(\alpha) & s(\beta) \\ c(\gamma)s(\alpha) + c(\alpha)s(\beta)s(\gamma) & c(\alpha)c(\gamma) - s(\alpha)s(\beta)s(\gamma) & -c(\beta)s(\gamma) \\ s(\alpha)s(\gamma) - c(\alpha)c(\gamma)s(\beta) & c(\alpha)s(\gamma) + c(\gamma)s(\alpha)s(\beta) & c(\beta)c(\gamma) \end{bmatrix} \tag{7}$$

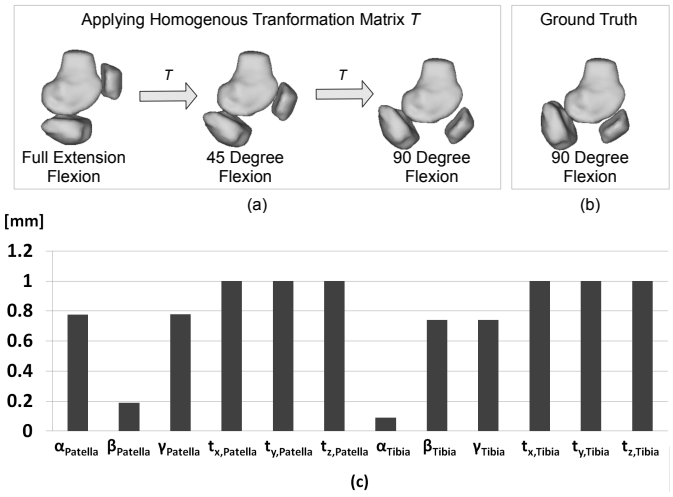

Fig. 4. The knee flexion is a nonlinear motion. The change from full extension to 45 degrees is described by a different homogeneous transformation matrix than from 45 degrees to 90 degrees. (a) Successive application of the 0–45 degree flexion matrix. (b) Application of the ground truth rigid transformation matrix 0–90 degree flexion. (c) Displacement of the mesh centre caused by an increase of one unit in each parameter of the global transformation matrix, 1 mm for translation and 1 deg for rotation.

The matrix $\mathbf{T}$ was the 4×4 homogeneous transform as in Eq. (6).

After the preprocessing alignment steps, an analysis of the linearity of the knee flexion and the dominant degrees of freedom was performed with the following findings:

- The anatomical knee flexion is a nonlinear transformation; moving from 45 degrees to 90 degrees is not described by the inverse matrix of moving from 45 degrees to full extension (Fig. 4). The nonlinearity here can be expressed mathematically as $f(\alpha)+f(\beta) \neq f(\alpha+\beta)$ and $f(k \cdot \alpha) \neq k \cdot f(\alpha)$, where f is a generalisation of the knee flexion function, α and β are knee flexion angles, and $k > 0$ is a constant.
- The dominant motion was identified from the parameters with the largest contribution towards the displacement of the patella and tibia mesh centres (Fig. 4). The flexion angle was primarily defined by a rotation about an axis at equal angle between the global x and z axis for the patella and y and z for the tibia, respectively. Additionally to the dominant rotation, there was significant twisting about the secondary axes y for patella and x for the tibia.

These findings proved the need for a general learning algorithm, which did not rely on the geometric bending of the knee at predefined degrees or on the linearity of the flexion. Moreover, the model should not simplify the number of degrees of freedom to the ones which give the most flexion, as important inaccuracies can sum up from the other secondary components.

Consequently, a subject-specific statistical flexion model was developed based on linear PCA of the parameters of an embedding function, i.e., the rigid transformation matrix. The mean was computed according to Eq. (8), whereas the covariance matrix was described by Eq. (9).

$$\bar{\mathbf{p}} = \frac{1}{N} \sum_{f \in Flexion} \mathbf{p}_f \tag{8}$$

$$\mathbf{S_p} = \frac{1}{N-1} \sum_{f \in Flexion} (\mathbf{p}_f - \bar{\mathbf{p}}) \cdot (\mathbf{p}_f - \bar{\mathbf{p}})^{\mathrm{T}} \tag{9}$$

The variable $\bar{\mathbf{p}}$ was the subject-specific average pose and $\mathbf{S_p}$ was the covariance matrix of the random variable $\mathbf{p}_f - \bar{\mathbf{p}}$. The normalisation constant N was the number of flexion angles in $Flexion$.

The PCA model contained only four initial shapes for each subject. In order to describe new shapes better, a larger training set was needed. In the next section, a method for artificially enlarging a small training set is proposed.

D. Enlargement of the Training Set

In a clinical setting for treatment of ruptured ACL, a small set of preoperative MR images of the knee are typically used to diagnose the area of intervention and plan the surgical procedure. For example, the MR data set may be limited to four stacks of images per patient, not enough to generate an accurate statistical model. The computed model would not be able to fit new shapes, even if they lay on the bending trajectory from full-extension to 90 degrees. This is due to the nonlinearity of the motion. Simple interpolation of the parameters with the highest contribution to the flexion (Fig. 4) would leave out important details, for example twisting about the secondary y axis for the patella and x axis for the tibia, resulting in an error outside of the allowable range of 1 mm [3].

The instantiation error of a model built from only four flexion angles was computed in four cross-validation cases for each subject and the median errors were 5.8 mm for patella, 4.8 mm for tibia, and 4.4 mm for the ACL insertion points on the tibia, largely above 1 mm and deeming the model unreliable.

Three modes of variation were generated from four shapes, according to Eq. (10) and (11); these are depicted in Fig. 5.

$$\mathbf{p}_{\mathrm{Lower},m} = \bar{\mathbf{p}} - 3 \cdot \sqrt{\lambda_m} \cdot \mathbf{u}_m \tag{10}$$

$$\mathbf{p}_{\mathrm{Upper},m} = \bar{\mathbf{p}} + 3 \cdot \sqrt{\lambda_m} \cdot \mathbf{u}_m \tag{11}$$

Here, λ_m was the m-th eigenvalue of the covariance matrix computed from the set of parameters $\mathbf{p}_f$, $f \in Flexion$, and $\mathbf{u}_m$ was the corresponding eigenvector. Due to the limited training set, the model not only yielded large instantiation errors, but also behaved very rigidly and generated intersecting invalid meshes such as the lower mode 1 in Fig. 5.

In light of these results, an enlargement of the training set for a more accurate statistical model was required. The enlargement method proposed in this paper acted on each parameter of the vector $\mathbf{p}$ separately, decoupling all degrees of freedom. Each subject-specific training set comprising 12 parameters for the four flexion angles was enlarged. The method was independent of the geometric angles of 0, 30, 45, and 90 degrees, only assuming a fairly widely spread space of the four observed variables.

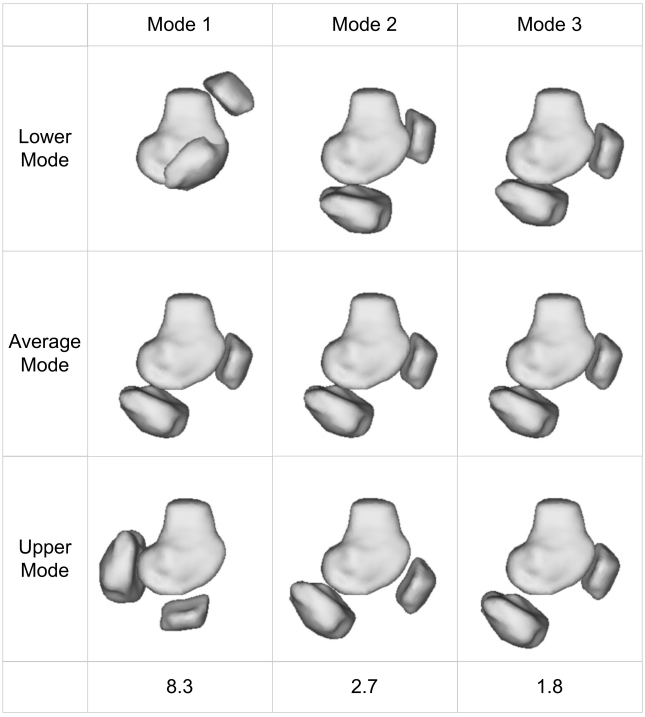

Fig. 5. Nonlinear PCA performed on concatenated vertices of all shapes of one subject. The meshes show the three modes of variation obtainable from four shapes, with a threefold standard deviation about the mean shape, as in Eq. (10) and (11). The model was too rigid and generated intersecting meshes, e.g. lower mode 1.

1) Piece-Wise Rigid Transformation Enlargement: Based on the adaptive-focus algorithm of Shen and Davatzikos [22] and the finite element enlargement first presented by Cootes and Taylor [21], a new method for enlarging the initial data set was developed. From only N shapes, the algorithm was able to generate $N \cdot 3^{12}$ additional meshes.

Firstly, the standard deviation of each parameter was computed as in Eq. (12) and concatenated in the standard deviation vector $\mathbf{s}$. This step was regarded as decoupling of the flexion parameters.

$$\mathbf{s} = \left(\frac{1}{N-1} \sum_{f \in Flexion} (\mathbf{p}_f - \bar{\mathbf{p}})^2 \right)^{\frac{1}{2}} \tag{12}$$

Secondly, all tertiary combinations of $\{-3s_i, 0, +3s_i\}$ for all 12 parameters $p_{i,f}, i = 1 \ldots 12, f \in Flexion$, were computed, so as to span a symmetric space around the average value of $p_{i,f}$, as in Eq. (13), where $f \in Flexion$ and $c_\mathrm{s} \in \{-3, 0, 3\}$, as shown in Fig. 6(a). This step yielded N^{12} new values about $\mathbf{p}_f$. Applying this algorithm to all initial shapes resulted in a total of $N \cdot 3^{12}$ meshes, with N the number of initial samples, i.e. 4 in the original subject-specific training set.

$$\mathbf{p}_{f_\mathrm{new}} = \mathbf{p}_f + c_\mathrm{s} \cdot \mathbf{s} \tag{13}$$

2) Spatial Validity of the Enlarged Training Set: The $\{-3s_i, 0, +3s_i\}$ shape generation, with s_i the standard deviation of parameter $\mathbf{p}_i$, kept the new objects in an anatomically possible pose to each other, about the mean which was previously established as a valid orientation of all bones. However, intersecting objects in the enlarged training set $\mathbf{p}_{f_\mathrm{new}}$ could still have been accepted without proper filtering.

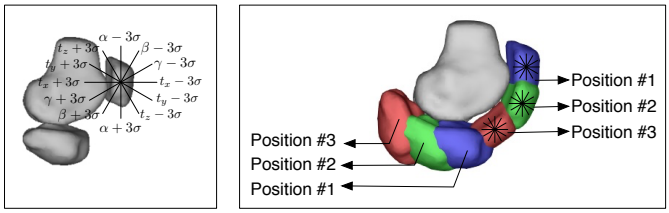

Fig. 6. At each knee flexion angle, the pose parameter set of the patella and the tibia was artificially enlarged. The resulting multi-shape objects were filtered with an intersection test. (a) The original shape was rigidly transformed via an artificially generated set of homogeneous parameters. Each parameter $p_{i,f}, i = 1 \ldots 12, f \in Flexion$, was changed in turn to $p_{i,f} - 3 \cdot s_i$ and $p_{i,f} + 3 \cdot s_i$ and all combinations were computed, resulting in 3^{12} vector values, where s_i is the standard deviation of parameter $\mathbf{p}_i$. (b) For cross-validation, each initial training set containing three shapes was enlarged with the non-rigid finite element method, resulting in $3 \cdot 3^{12}$ possible shapes, all based on 3 single shapes.

An exhaustive search in the 3D space was performed in order to check the overlaps between all combinations of femur, patella, and tibia triangular faces. The Interval Overlap Method [36] was implemented as a C++ library imported into MATLAB. The algorithm analysed the intersection of all pairs of planes, each plane including a triangle of either the full extension femur, or of the newly generated patella or tibia.

With the enlarged data set, $Flexion_\mathrm{enl}$, the new mean and covariance matrix were computed according to Eq. (14) and (15), where $\mathbf{p}_{f_\mathrm{enl}}$ were the sets of transformation parameters $\mathbf{p}_{f_\mathrm{new}}$ which generated non-intersecting meshes. With the new data set being much larger than the dimension of the vectors, the modes of variation were dictated by the space size of the parameters p_i, 12, and thus 11 modes being generated.

$$\bar{\mathbf{p}}_\mathrm{enl} = \frac{1}{N_\mathrm{enl}} \sum_{f_\mathrm{enl} \in Flexion_\mathrm{enl}} \mathbf{p}_{f_\mathrm{enl}} \tag{14}$$

$$\mathbf{S}_{\mathbf{p}_\mathrm{enl}} = \frac{1}{N_\mathrm{enl} - 1} \sum_{f_\mathrm{enl} \in Flexion_\mathrm{enl}} (\mathbf{p}_{f_\mathrm{enl}} - \bar{\mathbf{p}}_\mathrm{enl}) \cdot (\mathbf{p}_{f_\mathrm{enl}} - \bar{\mathbf{p}}_\mathrm{enl})^\mathrm{T} \tag{15}$$

where $\bar{\mathbf{p}}_\mathrm{enl}$ and $\mathbf{S}_{\mathbf{p}_\mathrm{enl}}$ were the new mean parameter vector and covariance matrix, respectively, and N_enl was the size of the enlarged training set.

III. Results

For each subject and each of the four flexion angles, the training set of the three remaining shapes was enlarged on a leave-one-out basis (Fig. 6(b)), resulting in $3 \cdot 3^{12}$ possible shapes for each of the 84 leave-one-out tests. The maximal shape set was then filtered for intersecting meshes with the Interval Overlap Method [36].

Fig. 7 compares the cross-validation results of using the initial three-shape training set and the enlarged training set for all subjects. Specific attention was paid to the instantiation error at the ACL attachment points. The global instantiation

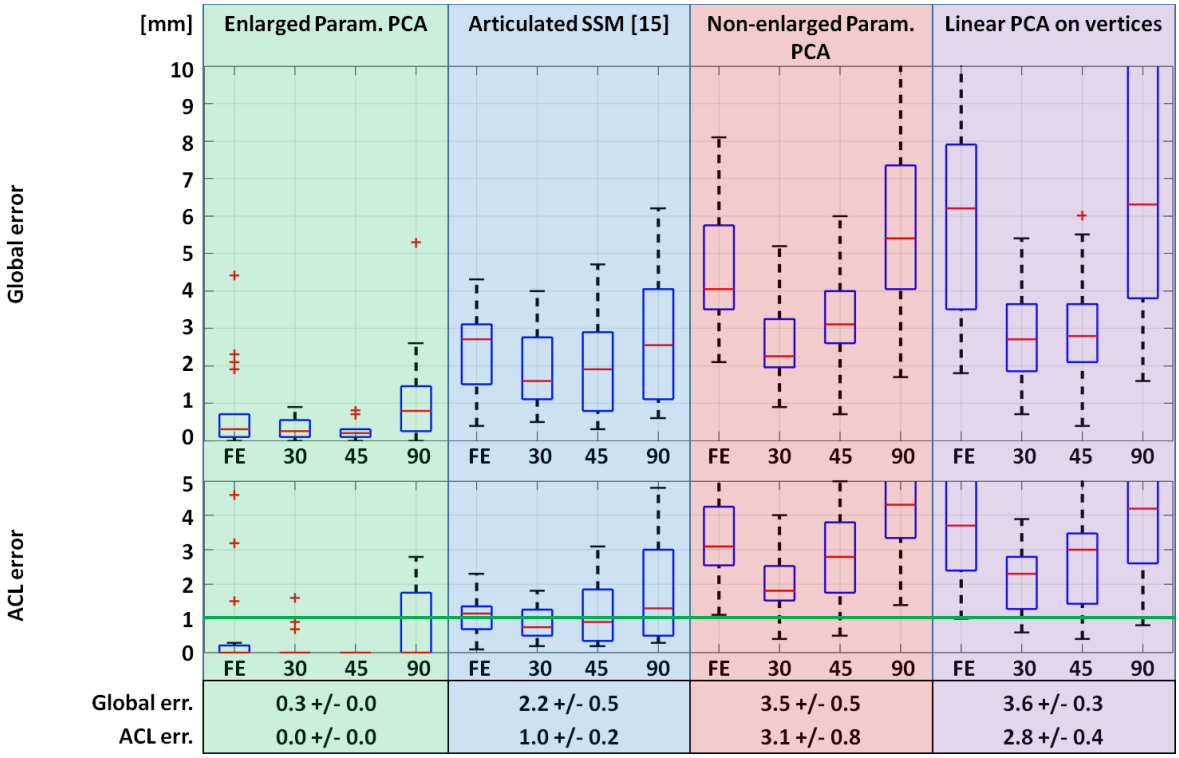

Fig. 7. Complete cross-validation results [mm] with median error over all subjects and flexion angles. The upper charts show the median errors over all surface vertices on patella and tibia in each of the flexion angles. The lower charts show the median error over the ACL insertion points. The box plots depict the median error (red line) and the 25-75 percentile interval. The whiskers extend to the most extreme data points not considered outliers, covering 99 % of the data. The median error at the ACL insertion points for Enlarged Parameter PCA was 0.0 mm, with only 11 values out of 84 beyond 1 mm (green line). The outliers (red crosses) are caused by the bias of the statistics, which drew the medians to 0.0 mm based on the large numbers of zero-value results. The tabled values underneath each method represent the cumulated global and ACL median errors +/- averages of the 25 and 75 percentiles, similar to the standard deviation of a normal distribution.

error was computed according to Eq. (16) and the local error at the ACL insertion points as in Eq. (17).

$$e_f = \frac{1}{n_{\text{Patella}} + n_{\text{Tibia}}} \sum_{s \in \{\text{Patella,Tibia}\}} \sum_{i=1}^{n_s} |\hat{\mathbf{R}}_{f,s} \cdot \mathbf{x}_{i,\text{FE},s} + \hat{\mathbf{t}}_{f,s} - \mathbf{x}_{i,f,s}| \tag{16}$$

$$e_{\text{ACL}_f} = \frac{1}{n_{\text{ACL}}} \sum_{i=1}^{n_{\text{ACL}}} |\hat{\mathbf{R}}_{f,\text{Tibia}} \cdot \mathbf{x}_{\text{ACL}_i,\text{FE,Tibia}} + \hat{\mathbf{t}}_{f,\text{Tibia}} - \mathbf{x}_{\text{ACL}_i,f,\text{Tibia}}| \tag{17}$$

The ACL error was calculated for the tibial insertions only, as the femur was fixed throughout the flexion. The estimated rotation matrix $\hat{\mathbf{R}}_{f,s}$ can be obtained from Eq. (7) by replacing with the instantiated parameters and the translation vector $\hat{\mathbf{t}}_{f,s}$ expressed as $[t_{\text{x},f,s}; t_{\text{y},f,s}; t_{\text{z},f,s}]$. The vector $\mathbf{x}_{i,f,s}$ is a 3D point describing the position of vertex i of the structure s at the flexion angle of f. For the ACL error computation, only the n_{ACL} tibia vertices which represented ACL insertion points $\mathbf{x}_{\text{ACL},f,\text{Tibia}}$ were taken into consideration.

The outliers in the box plots of Fig. 7 (red crosses) were caused by the imbalanced number of 0.0 mm errors which drew the statistics towards this value and excluded other non-zero values as outliers. Although their seemingly large number threatens the robustness of the proposed method, the error at the points of interest, i.e. the ACL osseous insertions, remains under 1 mm (green line in Fig. 7) in 73 out of 84 cross-validation studies. The outliers distribution is as follows: 4 at FE, 1 at 30 degrees, and 6 at 90 degrees.

These statistics show reduced robustness at the extreme angles of full extension and 90 degrees, where the difference to the closest training data of 30 and 45 degrees is large not only along the bending axis, but also in the parameter space. It can be inferred that with a better and more uniformly distributed angle sampling strategy, better results can be achieved.

The proposed method was also tested against the articulated joint reconstruction in [15]. According to the latter, the knee joint of each patient had a fixed flexion-extension axis in the femur. This axis was defined by its unit vector $\mathbf{d}=(d_\text{x}, d_\text{y}, d_\text{z})^\text{T}$. Furthermore, the knee kinematics about this axis were simplified to an articulated motion composed of the rotation $\mathbf{R}_{f,s}(\mathbf{d}, \Theta_{f,s})$ of the structure $s \in Structure$ by the angle $\Theta_{f,s}$ (Eq. 16), plus a 3D translation for each bone, $\mathbf{t}_{f,s} = [t_{\text{x},f,s}; t_{\text{y},f,s}; t_{\text{z},f,s}]^\text{T}$, where $f \in Flexion$.

The articulated knee motion parameters $\mathbf{d}$, $\Theta_{f,s}$, and $\mathbf{t}_{f,s}$ at each pose were estimated independently of the other angles by solving the following non-linear least-squares fitting problem with a Levenberg-Marquardt optimizer:

$$\underset{\mathbf{d},\Theta_{f,s},t_{f,s}}{\arg\min} \sum_{s \in Structure} \sum_{i=1}^{n_{\text{V}_s}} \|\mathbf{R}_{f,s}(\mathbf{d}, \Theta_{f,s}) \cdot \mathbf{v}_{\text{FE,s},i} + \mathbf{t}_{f,s} - \mathbf{v}_{f,s,i}\|$$

where $\mathbf{v}_{\text{FE},s,i}, i = 1 \ldots n_{\text{V}_s}$ were the vertices on the surface

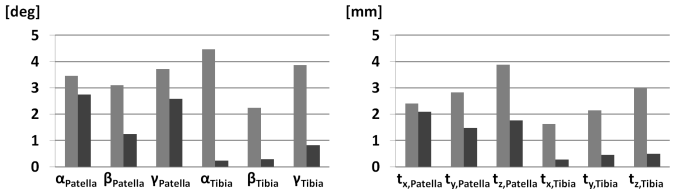

Fig. 8. Instantiation error of the homogeneous transformation parameters. Left chart – rotation parameters [deg]. Right chart – translation parameters [mm]. Light grey – no enlargement. Dark grey – enlargement.

model of the structure $s \in Structure$ at the reference position of full extension, with n_{V_s} the number of vertices in structure s.

The comparative results of the optimisation for each subject and each flexion angle are presented in Fig. 7. The median error in both the global bone instantiation and at the local ACL attachment proves a better fitting performance of the algorithm presented in this paper compared to [15]. A Kruskal-Wallis test was performed to infer statistical difference between the results of the proposed method and the ones from [15], as well as between the results of the proposed method and the linear PCA. The significance level of the statistical test was computed at 1 % in MATLAB's implementation of the Kruskal-Wallis test. The result proved that the median of the proposed method was not equal to the median in either of the other two methods compared against. Since their medians were higher, it was concluded that the error over all subjects for the enlarged parameter PCA was statistically significantly lower.

For a statistical model of flexion, of particular interest were also the fitting errors of the rigid transformation itself, p_i, where $p_2 = \alpha_{\text{Patella}}$, $p_3 = \gamma_{\text{Patella}}$, $p_8 = \beta_{\text{Tibia}}$, and $p_9 = \gamma_{\text{Tibia}}$ played the most important role as parameters for the dominant motion (Fig. 4). Fig. 8 shows the median of the cross-validation results over all subjects and all flexion angles with and without enlargement of the training set. For the rotation parameters, the error is given in degrees and for translational parameters in mm.

A blind validation of the flexion model was performed for 60, 70, and 80 degree flexion of the tibia in the CLA 10 knee phantom. The training data consisted of the FE, 30, 45, and 90 degree meshes. The global tibial pose instantiation error was 0.0, 0.8, and 0.7 mm, respectively, while at the ACL insertion points it was 0.0, 0.8, and 1.1 mm, respectively. The low errors confirmed that the model performed better when the difference in angles along the bending trajectory was smaller and the data was more uniformly sampled.

In addition to the validation of the flexion model, a similar framework was built to test the accuracy in tracking twisting angles. The original data set included scans of the CLA 10 knee phantom at FE, 30, 45, and 60 degrees flexion, each twisted additionally by 5 degrees either side of the tibial axis. The training set enlargement was performed for each flexion angle separately from the others, so that the modelled motion would be limited to the twisting and invariant to flexion. Twelve leave-one-out enlargements and validation tests were performed, one for every position. The median error of the enlarged model was 1.6 mm, with the local error at the ACL insertion points averaging 1.1 mm. The enlarged twisting model was able to describe modes of variation as pictured in Fig. 9.

	Mode 1	Mode 2	Mode 3	Mode 4	Mode 5
Lower Mode	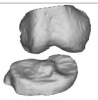				
Average Mode					
Upper Mode		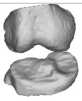	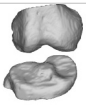		
Mode Variance	137.2	60.4	20.4	3.7	3.6

Fig. 9. Modes of variation described by the twisting model, starting from three shapes, at 30 degrees with no twist and at 30 degrees with twist of 5 degrees either side of the tibial axis.

IV. Discussion

In this paper, we have presented a new model for intra-operative pose estimation based on the statistical analysis of the homogeneous transformation parameters between two poses of the same object. The training set was enlarged using piece-wise rigid deformations of the motion parameter vectors, creating additional poses for learning. The statistical flexion model combined with the training set enlargement was assessed in 84 cross-validation and 3 blind validation tests.

A subject-specific flexion model can be seen as the pre-requisite for augmented reality in arthroscopic ACL repair. While the diagnostic preoperative scanning can include only a sparse set of bending and flexion angles, the proposed enlarged statistical model of transformation parameters could instantiate new bone poses intraoperatively. In a typical scenario, the arthroscopic view could capture a new pose of the anatomy. The missing surface and the ACL insertions could be reconstructed by constraining the flexion model instantiation according to correspondences on the visuallsed patch.

It should be noted that despite the median error being lower than that of the other methods, the enlarged PCA on the transformation matrix parameters yielded 11 outliers outside

$$\mathbf{R}_{f,s}(\mathbf{d},\Theta_{f,s}) = \begin{bmatrix} c(\Theta_{f,s}) + d_{\mathrm{x}}^2(1-c(\Theta_{f,s})) & d_{\mathrm{x}}d_{\mathrm{y}}(1-c(\Theta_{f,s})) - d_{\mathrm{z}}s(\Theta_{f,s}) & d_{\mathrm{x}}d_{\mathrm{z}}(1-c(\Theta_{f,s})) + d_{\mathrm{y}}s(\Theta_{f,s}) \\ d_{\mathrm{x}}d_{\mathrm{y}}(1-c(\Theta_{f,s})) + d_{\mathrm{z}}s(\Theta_{f,s}) & c(\Theta_{f,s}) + d_{\mathrm{y}}^2(1-c(\Theta_{f,s})) & d_{\mathrm{y}}d_{\mathrm{z}}(1-c(\Theta_{f,s})) - d_{\mathrm{x}}s(\Theta_{f,s}) \\ d_{\mathrm{x}}d_{\mathrm{z}}(1-c(\Theta_{f,s})) - d_{\mathrm{y}}s(\Theta_{f,s}) & d_{\mathrm{y}}d_{\mathrm{z}}(1-c(\Theta_{f,s})) + d_{\mathrm{x}}s(\Theta_{f,s}) & c(\Theta_{f,s}) + d_{\mathrm{z}}^2(1-c(\Theta_{f,s})) \end{bmatrix} \quad (16)$$

the 25–75 percentile interval. This is shown by the red crosses in Fig. 7. The outliers were also an issue for the linear PCA on vertices and for the non-enlarged PCA on transformation matrix parameters, which suggested decreased robustness of PCA in this case.

However, the robustness of the algorithm was shown to increase with the MRI resolution. When considering the number of cross-validation errors at the ACL attachment, the ratio of errors below 1 mm to errors above 1 mm increased from 2.5 (first seven subjects, MRI slice thickness 3 mm) to 6.42 (last thirteen subjects, MRI slice thickness 0.6 mm). The higher imaging resolution allows for better alignment along the twisting axis in addition to the dominant flexion trajectory. Thus, the proposed method is superior in performance to single-axis motion models such as [15].

Due to the nonuniform distribution of the cross-validation results, there was a narrow interval around the 0.0 mm median. This caused an exclusion of other values as outliers, despite being in the 1 mm accuracy band. From the 11 outliers in Fig. 7, only 6 were beyond the 1 mm mark. The method thus yielded submillimetre accuracy in 78 out of 84 studies and statistically significant lower medians than all other comparison methods. The merit can be attributed to the piece-wise rigid transformation enlargement, as can be seen from a comparison with the non-enlarged method. Regarding the sampling angles used in the model, the blind validation on intermediate meshes of 60, 70, and 80 degrees showed potential in pose instantiations for angles close to the ones in the training set of FE, 30, 45, and 90 degrees, but poorer results for cross-validation on extremes such as FE and 90 degrees. Taking into consideration that the extremes can be acquired preoperatively and included in the training set, the proposed method results can produce submillimetre pose fitting accuracy.

The twisting model based on knee flexion scans was computed from flexion invariant shapes by enlarging the data set within each twisting angle. Despite the intention of emphasizing only the twisting, the training set enlargement method acts on secondary pose axes as well, thus influencing the flexion. This proves that the two knee joint pose changes are coupled and should be studied together in a complex flexion-twisting model as proposed.

The statistical flexion model presented in this paper is generated from intact ACL subjects to demonstrate the feasibility of the method. Our next step is to assess the method for ACL reconstruction of patients. It is worth noting that the multi-object shape modelling approach presented in this paper only relies on the pose of rigid bodies. The shape itself and especially the knee kinematics involve a high contribution of the intact ACL and thus it can be understood that there is an implicit model of ACL within the rigid multi-object shape. Nevertheless, even with torn ACL, the function is supported by the adjacent soft tissue, such as muscles and other ligaments and tendons. With a subject-specific preoperative model, the kinematic pattern of any soft tissue can be incorporated. The only prerequisite is that the flexion angles in the training set are reproducible.

V. Conclusion

In summary, a new combination of statistical models and piece-wise rigid deformation enlargement was presented. The training set of the model comprising the parameters of two rigid transformation matrices was enlarged by local changes in the motion parameter vector. Subsequently, a statistical model of flexion based on anatomic geodesic analysis was generated.

Although the method used meshes from MRI scans in four predefined flexion angles of 0, 30, 45, and 90 degrees, it was not dependent on the geometric angles built by the femoral and tibial axes, but only on a good spread of the values in space. A potential future development point is studying the accuracy with only three initial meshes and finding the necessary spread in order to create a good initial training set.

The added value of the proposed approach was clearly demonstrated by the phantom study using a set of simultaneously twisted and flexed phantom knee scans. Twisting is an important component in the motion of injured ACL patients. In this paper, the twist was quantified and modelled for the first time to our knowledge.

Moreover, the proposed training set enlargement strategy offered a mathematically viable method to bring the model's fitting accuracy in the 1 mm error band and thus render it clinically relevant. This improvement can be inferred from Fig. 7. The PCA on the parameters of the rigid transformation matrix was itself the foundation for applying this enlargement method, by moving the contour representation onto a manifold where statistical analysis can be performed.

In conclusion, a new combination of a statistical model based on anatomic geodesic decomposition and of a piece-wise rigid training set enlargement for intraoperative guidance of ACL repair was proposed. Taking into account the submillimetre accuracy achieved in the validation tests, the proposed method has clinical potential in reducing the invasiveness of intraoperative tracking for orthopaedic procedures.

Acknowledgment

The authors would like to thank Mr Konrad Leibrandt and Dr Jindong Liu, The Hamlyn Centre for Robotic Surgery, London, UK, for providing the mesh collision library and for the help with the phantom setup, respectively, Mr Mohammed Mohammed, Aspetar Orthopaedic and Sports Medicine Hospital, Doha, Qatar, for the assistance with data collection, and Ms Sally Elgazar, Qatar Robotic Surgery Centre, Qatar Science & Technology Park, Doha, Qatar, for the help with MRI segmentation.

References

[1] NHS, "Knee ligament surgery," last visited 19/08/2014. [Online]. Available: http://www.nhs.uk/conditions/Repairtotendon/Pages/Introduction.aspx

[2] H. Ikeda, T. Muneta, and S. Niga, "The long-term effects of tibial drill hole position on the outcome of anterior cruciate ligament reconstruction," *Arthroscopy*, vol. 15, no. 3, pp. 287–291, Apr 1999.

[3] F. Picard, A. M. DiGioia, and J. Moody, "Accuracy in tunnel placement for ACL reconstruction. Comparison of traditional arthroscopic and computer-assisted navigation techniques," *Comput. Aided Surg.*, vol. 6, no. 5, pp. 279–289, 2001.

[4] M. Degenhart, "Computer-navigated ACL reconstruction with the OrthoPilot," *Surg Technol Int*, vol. 12, pp. 245–251, 2004.

[5] A. Burkart, R. E. Debski, and P. J. McMahon, "Precision of ACL tunnel placement using traditional and robotic techniques," *Comput. Aided Surg.*, vol. 6, no. 5, pp. 270–278, 2001.
[6] D. E. Meuffels, M. Reijman, and R. J. Scholten, "Computer assisted surgery for knee ligament reconstruction," *Cochrane Database Syst Rev*, no. 6, p. CD007601, 2011.
[7] P. Bonutti, D. Dethmers, and J. B. Stiehl, "Case report : femoral shaft fracture resulting from femoral tracker placement in navigated TKA," *Clin. Orthop. Relat. Res.*, vol. 466, no. 6, pp. 1499–1502, Jun 2008.
[8] T. Cootes, C. Taylor, and D. Cooper, "Active shape models–their training and application," *Computer Vision and Image Understanding*, vol. 61, no. 1, pp. 38–59, Jan 1995.
[9] M. Kass, A. Witkin, and D. Terzopoulos, "Snakes: active contour models," *Int J Comp Vision*, pp. 321–331, 1987.
[10] K. Stark and S. Fuchs, "A method for tracking the pose of known 3-D objects based on an active contour model," *ICPR*, vol. 1, pp. 905–909, 1996.
[11] M. Leventon, E. Grimson, and O. Faugeras, "Statistical shape influence in geodesic active contours," *CVPR*, vol. 1, pp. 316–323, 2000.
[12] M. Fleute, S. Lavallee, and R. Julliard, "Incorporating a statistically based shape model into a system for computer-assisted anterior cruciate ligament surgery," *Med Image Anal*, vol. 3, no. 3, pp. 209–222, Sep 1999.
[13] N. Baka, B. L. Kaptein, and J. E. Giphart, "Evaluation of automated statistical shape model based knee kinematics from biplane fluoroscopy," *J Biomech*, vol. 47, no. 1, pp. 122–129, Jan 2014.
[14] C. K. Fitzpatrick, M. A. Baldwin, and P. J. Laz, "Development of a statistical shape model of the patellofemoral joint for investigating relationships between shape and function," *J Biomech*, vol. 44, no. 13, pp. 2446–2452, Sep 2011.
[15] S. Balestra, S. Schumann, and J. Heverhagen, "Articulated statistical shape model-based 2D-3D reconstruction of a hip joint," *IPCAI (LNCS)*, vol. 8498, pp. 128–137, 2014.
[16] M. Scholz and R. Vigario, "Nonlinear PCA: a new hierarchical approach," *10th European Symposium on Artificial Neural Networks, ESANN*, pp. 439–444, Apr 2002.
[17] T. Fletcher, C. Lu, and S. Pizer, "Principal geodesic analysis for the study of nonlinear statistics of shape," *Transactions on Medical Imaging*, vol. 23, no. 8, pp. 995–1005, Aug 2004.
[18] S. Jung, M. Foskey, and J. Marron, "Principal arc analysis on direct product manifolds," *Annals of Applied Statistics*, vol. 5, no. 1, pp. 578–603, 2011.
[19] M. Bossa and S. Olmos, "Multi-object statistical pose+shape models," *Biomedical Imaging: From Nano to Macro*, pp. 1204–1207, Apr 2007.
[20] M. Zhang and T. Fletcher, "Probabilistic Principal Geodesic Analysis," *Neural Information Processing Systems*, Aug 2013.
[21] T. Cootes and C. Taylor, "Combining point distribution models with shape models based on finite element analysis," *Image and Vision Computing*, vol. 13, no. 5, pp. 403–409, Jun 1995.
[22] D. Shen, E. Herskovits, and C. Davatzikos, "An adaptive-focus statistical shape model for segmentation and shape modeling of 3-D brain structures," *Transactions on Medical Imaging*, vol. 20, no. 4, pp. 257–270, Apr 2001.
[23] C. Davatzikos, X. Tao, and D. Shen, "Hierarchical active shape models, using the wavelet transform," *IEEE TMI*, vol. 22, no. 3, pp. 414–423, Mar 2003.
[24] J. Loetjoenen, K. Antila, and E. Lamminmaeki, "Artificial enlargement of a training set for statistical shape models: application to cardiac images," *FIMH (LNCS)*, vol. 3504, pp. 92–101, 2005.
[25] T. Toelli, J. Koikkalainen, and K. Lauerma, "Artificially enlarged training set in image segmentation," *MICCAI (LNCS)*, vol. 4190, pp. 75–82, 2006.
[26] A. Merchant, R. Mercer, R. Jacobsen, and C. Cool, "Roentgenographic analysis of patellofemoral congruence," *Bone Joint Surg Am*, vol. 7, no. 56, pp. 1391–1396, 1974.
[27] M. Miller and S. Wiesel, Eds., *Operative techniques in sports medicine surgery*. Lippincott Williams & Wilkins, 2011.
[28] M. Miller and S. Thompson, Eds., *Orthopaedic sports medicine*. DeLee & Drez's, 2015.
[29] A. Rosset, L. Spadola, and O. Ratib, "OsiriX: an open-source software for navigating in multidimensional DICOM images," *Digital imaging*, vol. 17, no. 3, pp. 205–216, 2004.
[30] W. Lorensen and H. Cline, "Marching cubes: A high resolution 3D surface construction algorithm," *SIGGRAPH*, vol. 21, no. 4, pp. 163–169, July 1987.
[31] O. Sorkine, D. Cohen-Or, and Y. Lipman, "Laplacian Surface Editing," *Symposium on Geometry Processing*, pp. 175–184, 2004.
[32] P. Cignoni, M. Corsini, and G. Ranzuglia, "MeshLab: an open-source 3D mesh processing system," *ERCIM news, Year =*.
[33] "Normal ranges of joint motion," http://web.mit.edu/tkd/stretch/stretching_8.html#SEC91, accessed: 27/11/2015.
[34] P. Besl and N. McKay, "A method for registration of 3-D shapes," *IEEE Trans. on Pattern Analysis and Machine Intelligence*, vol. 14, no. 2, pp. 239–256, February 1992.
[35] B. Horn, H. Hilden, and S. Negahdaripour, "Closed-form solution of absolute orientation using orthonormal matrices," *J Opt Soc Am A*, vol. 5, no. 7, pp. 1127–1135, Jul 1988.
[36] T. Moeller, "A fast triangle-triangle intersection test," *Graphics tools*, vol. 2, no. 2, pp. 25–30, 1997.